Spectral Albedo Estimation of Snow Covers in Pakistan Using Landsat Data

Mohsin Jamil Butt[1] · Mazen Ebraheem Assiri[1] · Ahmed Waqas[2]

Abstract

Accurate snow spectral albedo measurements from satellite data can essentially help to determine the changes over the snow surface area. In the current study, spectral snow albedo is measured over the northern region of Pakistan using spatio-temporal imagery datasets taken by Landsat satellite series equipped with TM and ETM+ sensors. An Automatic Cloud Cover Assessment (ACCA) algorithm is used to mask cloudy pixels from further processing. Furthermore, an image independent model, Second Simulation of the Satellite Signal in the Solar Spectrum (6S) is used in the current research work to atmospherically correct the satellite data. The snow cover albedo of northern Pakistan is estimated using pixel values prior to correction, ACCA output values, and 6S model output values. The results of the study show that highest albedo values are estimated using Landsat band 4 data with albedo model. The results of the study also show that the albedo values measured (band 4) in the year 1992 (0.989) are reduced in the year 2000 (0.931). It is expected that the results of the study could be utilized to predict climatic variations for spring runoff estimation.

Keywords Albedo · MSS · TM · ETM+ · ACCA · 6S

1 Introduction

Surface albedo is an essential climate variable (Bhutiyani et al. 2010; Schaaf et al. 2008) and is important to understand the lower boundary for atmospheric radiative transfer (Hu et al. 1999). For climate models, accurate global estimations of terrestrial albedo for all surface types during all seasons are required (Oleson et al. 2003; Ollinger et al. 2008; Roesch et al. 2004; Tian et al. 2004). Graversen and Wang (2009) reported that the surface-temperature response in the Arctic area is amplified about 33% by surface albedo feedback. Fletcher et al. (2009) demonstrated that in projections of the circulation response to climate change on average 5–10% of the intermodal spread is linearly related to the surface snow albedo feedback strength. In another study, Yang et al. (2001) reported that North American surface climate anomalies related to ENSO (El Nino–Southern Oscillation) is greatly enhanced by local snow-albedo feedback. Similarly, Déry and Brown (2007) showed that over northern latitudes the increased poleward retreat of the spring continental snow cover is consistent with an enhanced snow albedo feedback, whilst Souma and Wang (2010) has linked snow albedo with variations in the Asian summer monsoon rainfall. Earlier, scientists have used Radiation Budget Experiment (ERBE) radiometer (Li and Garand 1994) and Advanced Very High-Resolution Radiometer (Csiszar and Gutman 1999) satellite to produce global albedo datasets. The current albedo products are available from a number of satellite systems including Multiangle Imaging Spectro-Radiometer (MISR), Polarization and Directionality of the Earth's Reflectances (POLDER), Meteosat Second Generation (MSG) Spinning Enhanced Visible and Infrared Imager (SEVIRI) and Moderate Resolution Imaging Specroradiometer (MODIS).

Snow has the highest reflective nature combined with its large surface coverage. As a result, snow reflects a very high percentage of incoming solar radiations than snow-free surfaces in the visible portion of electromagnetic radiation (Srinivasulu and Kulkarni 2004). For fresh snow, the percentage reflectance of incoming solar radiation is more than

✉ Mohsin Jamil Butt
   mbutt@kau.edu.sa

[1] Department of Meteorology, Faculty of Meteorology, Environment and Arid Land Agriculture, King Abdulaziz University, Jeddah, Saudi Arabia

[2] Department of Meteorology, COMSATS University, Islamabad, Pakistan

90%, which drops to less than 40%, for the surface weathered and dirty snow (Hall and Martinec 1985). In addition, snow cover area affects the local and global climate and its behavior is considered an indicative of climate change (Gupta et al. 2007; Snehmani et al. 2016). The snow cover area plays a vital role in regional climate over mid-latitudes (Xiao et al. 2001). Current climate changes are mainly associated with the variation in the air temperature. The mean annual air temperatures rose dramatically in the 20th century (IPCC 2013). This trend intensified at the end of the last century and the areas of glacial ice coverage strongly diminished in many parts of the world (Haeberli 2004; Maisch 2000; Kääb et al. 2002; Khromova et al. 2003; Paul et al. 2004a, b; Robinson et al. 2014). Thus, the snow albedo has a strong positive feedback in the surface–atmosphere system (Viterbo and Betts 1999) whilst, high-quality global surface albedo is needed to further explore snow-albedo feedback impacts (Qu and Hall 2007). Snow covers are also responsible for more than 80% of the total fresh water on Earth (Dozier 1989). The resulting runoff from the snow and glacier melt supplies water for irrigation, hydro-electrical power generation and other human enterprises (Kaser et al. 2010; Joshi et al. 2015; Shukla et al. 2017; Thayyen and Gergan 2010; Thayyen and Dimri 2018). An ability to calculate snow albedo is therefore important for predicting seasonal snowmelt and runoff rates (Stigter et al. 2017) as well as for understanding the growth and decay of snowfields, which in turn affect not only the global energy budget (Kukla and Kukla 1974) but also very important for related disaster management issues (Immerzeel et al. 2010; Haeberli et al. 2014). Ground-based measurements can provide excellent temporal data on snow albedo however, their spatial coverage is limited. Furthermore, due to the seasonal variation, snow albedo varies considerably spatially (Knap et al. 1999) and thus ground-based measurement of snow albedo is not suitable for larger areas (Greuell and de Wildt 1999).

Satellite remote sensing has opened the possibility of data acquisition as well as has offered a broad view of surface albedo at the larger spatial and temporal scales as compared with ground data (Dozier 1989; Parajka et al. 2010; Paudel and Andersen 2011; Snehmani et al. 2015;

Tekeli et al. 2016; Rathore et al. 2018). Snow albedo in the visible wavelengths is sensitive to contamination but not to grain size, whereas it is more sensitive to the grain size than contaminants in the near-infrared wavelengths (Dozier 1989). Cloud removal techniques and algorithms have been developed for various satellite to improve remote sensing data interpretation and application (Gao et al. 2010; Hall et al. 2010; Paudel and Andersen 2011; López-Burgos et al. 2013; Cheng et al. 2014; Li et al. 2014; Wang et al. 2014). In Pakistan, some of the permanent snow features in the form of glaciers exist in HKH (Hindukush, Karakoram, and Himalaya) region. A very little research has been done in the past to highlight the importance of permanent snow features in the HKH region (Kulkarni et al. 2011; Dobhal et al. 2013; Kasturirangan et al. 2013). For example, Butt (2012) estimated snow characteristics by applying Normalized Difference Snow Index (NDSI), Snow Contamination Index (SCI), and Snow Grainsize Index (SGI) on Landsat ETM+ data for the year 2003 over the HKH region. The results of the study indicate that approximately 99.8% snow in the HKH region is least contaminated with 94.5% area has fine snow grain size. In another study, Butt (2013) prepared snow zonation of HKH region using Landsat ETM+ data and classify snow into six different classes, that is, clean surface of glaciers (10.78%), ice with dust (10.02%), wet snow (15.15%), snow area at high altitudes (26.87%), snow area at low altitudes (28.01%), and debris covered ice (9.12%) near peaks of the mountains.

The current study, therefore, focused to use satellite data to measure the spectral albedo of snow in HKH region of Pakistan. Satellite data from Landsat TM and ETM+ sensors were acquired whilst meteorological data was retrieved from Pakistan Meteorological Department (PMD). Snow albedo is retrieved in this study by directly using albedo model (Eq. 2) as well as after applying ACCA and 6S models for the removal of clouds and atmospheric correction, respectively. The ACCA algorithm eliminated clouds and dark pixels using several consecutive filters (Table 1).

Table 1 ACCA filters used with threshold values

No.	Filter	Function
1	Brightness threshold: B3 > 0.08	Eliminates dark images
2	Normalized Difference Snow Index (NDSI): $\text{NDSI} = \left(\frac{\text{Band2} - \text{Band5}}{\text{Band2} + \text{Band5}} \right) < 0.7$	Eliminates many types of snow
3	Temperature threshold: B6 < 300 K	Eliminates warm image features
4	Band 5/6 composite: $(1 - \text{B5}) \times \text{B6} < 225$	Eliminates numerous categories including ice
5	Band 4/3 ratio: B4/B3 < 2.0	Eliminates bright vegetation and soil
6	Band 4/2 ratio: B4/B2 < 2.0	Eliminates ambiguous features
7	Band 4/5 ratio: B4/B5 > 1.0	Eliminates rocks and desert

2 Study Area

The Northern area of Pakistan extends from 31.4°N to 36.8°N latitude and from 69.16°E to 74.7°E longitude. The mountainous regions in northern Pakistan have the snow covers for maximum periods (some of them are permanent) of the year (Smith and Bookhagen 2018). The study area in current research lies within the three mountainous regions, that is, Hindukush, Karakoram, and Himalaya that consists of the longest glaciers (outside polar zone) and the world's highest mountain peaks. It is the complexity of the study area that require using satellite remote sensing techniques (SAC 2016) for the measurements of snow albedo. The main study area (approximately 5689.81 km^2) used in this research is the Indus catchments comprising the spatial coverage of Mansehra, Batagram, Muzaffarabad, Swat and adjoining regions as shown in Fig. 1. Climate of HKH region experience temperate to alpine climate (winter and summers are dominant seasons) from low to high elevation (Grünewald et al. 2014; Gurung et al. 2017) and is highly influenced by monsoon (Dimri and Chevuturi, 2016) with heavy snowfall during the winter (November, December, January) and spring (February, March, and April) months (Dimri and Dash 2012; Negi et al. 2018). More than two-third of the annual flow through the rivers of the Indus Basin is derived from the melting of snow/glacier in the mountainous catchments areas of northern Pakistan.

3 Materials and Methods

3.1 Data Acquisition

The main focus of the current study is to use satellite data to measure the spectral albedo of snow in HKH region of Pakistan. The persistent bad weather condition in the region is one of the major difficulty while acquiring the cloud-free imagery of the study area. Therefore, an attempt was made to use images in almost no cloud conditions. In addition, the focus is made to use the near similar atmospheric and seasonal condition of all the acquired scenes (Liang et al. 2001). Thus, satellite data from Landsat TM and ETM+ sensors were acquired for the years 1992, 1998, and 2000, whilst meteorological data was retrieved from Pakistan Meteorological Department (PMD). There are 4 PMD ground stations (Astore, Bunji, Chilas, and Gilgit) that are located within the study area. These stations started to record meteorological data in different years. For example, PMD station at Gilgit started recording data from the year 1947 whilst the other stations started to record data from the year 1954. Thus, historical meteorological data from four weather stations exist in the study area are obtained from PMD.

3.2 Image Processing

Geometric correction on all the Landsat images used in this study was performed by re-projecting the images into WGS-84 (World Geodetic System 1984) ellipsoid, using north zone 43 of the UTM projection. The main advantage of the process is that it does not deform the original image (Snyder 1987). Ground Control Points (GCP) of the study area were acquired using Global Positioning System (GPS) device to perform the accurate geo-referencing of all the Landsat images. First order polynomial model and nearest-neighbor re-sampling method were applied to minimize the geometric and radiometric distortions in ERDAS imagine software.

The ability to detect quantified changes in the Earth's environment and its global energy balance depends on the satellite sensors that can provide calibrated consistent measurement of the Earth surface features (Chander and Markham 2003). Each object reflects energy differently in

Fig. 1 Selected study area of Northern Pakistan (red rectangle)
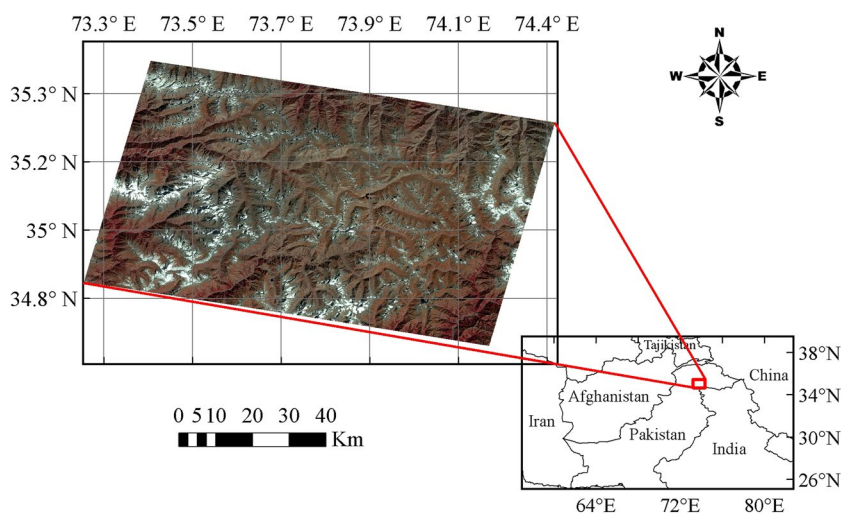
various parts of electromagnetic spectrum. This energy is normally represented in digital number (DN) depending on the calibration of the sensor (Srinivasulu and Kulkarni 2004). The pixel brightness values of TM and ETM+ bands 1, 2, 3, and 4 are converted into top of atmosphere (TOA) reflectance. Chander and Markham (2003) described detailed procedure for reflectance calculation. The image data is needed to be converted into TOA radiance before applying the actual algorithm. Equation 1 is used to convert and calibrate DN values to radiance values (Chander and Markham 2003):

$$L_\lambda = G_{\text{rescale}} \times Q_{\text{cal}} + B_{\text{rescale}}, \tag{1}$$

where L_λ = spectral radiance at the sensor's aperture in W/(m² sr μm), Q_{cal} = quantized calibrated pixel value in DNs, G_{rescale} and B_{rescale} = band specific rescaling factors given as;

$$G_{rescale} = \left(\frac{\text{LMAX}_\lambda - \text{LMIN}_\lambda}{Q_{\text{cal\_max}}} \right),$$

$$B_{\text{rescale}} = \text{LMIN}_\lambda,$$

where $Q_{\text{cal\_max}}$ = maximum quantized calibrated pixel value corresponding to LMAX_λ, LMIN_λ = spectral radiance that is scaled to $Q_{\text{cal\_min}}$ in W/(m² sr μm), LMAX_λ = spectral radiance that is scaled to $Q_{\text{cal\_max}}$ in W/(m² sr μm).

3.3 Methodology

A model is used to calculate planetary albedo on the monochromatic basis for each Landsat TM and ETM+ visible and near-infrared bands (bands 1, 2, 3, 4, 5, and 7). This model is based on the conversion of digital satellite numbers to radiance to be used for the albedo measurement. Additionally, the outputs obtained from ACCA algorithm and 6S models are also used to determine the snow albedo values. The flow chart diagram of methodology is given in Fig. 2. The results based on satellite images of three different dates are then manipulated to understand the temporal status of seasonal snow condition. In the current research, Mauro Antunes 6S atmospheric model improved by Zhang et al. (2012) has been used for atmospheric correction. This model is applicable to the raw 8-bit images. Similarly, ACCA algorithm that can successfully work to elimination cloudy areas in an image is applied in the current study. The algorithm constitutes a series of different filters with certain specified thresholds. This algorithm follows a continuous pattern removing clouds from the images using different thresholds. In the current research, it is intended to make the observation cloud free as much as possible so that accurate estimation of snow albedo can be attained. Therefore, cloud masking is accomplished using seven filters with specific functions as described in Table 1. In this assessment, the filter addressing the separation of warm and cold clouds is not used in current work. The reflectance values obtained after the implementation of filters were converted to spectral albedo for spectral profile analysis. Spectral albedo (ratio of the upwelling irradiance to the downward irradiance at the solar zenith angle θ) model modified by Chander et al. (2009), as given in Eq. (2), is used in this study. The model is independent of viewing angle for upwelling radiance and is used only

Fig. 2 Flow chart diagram of methodology
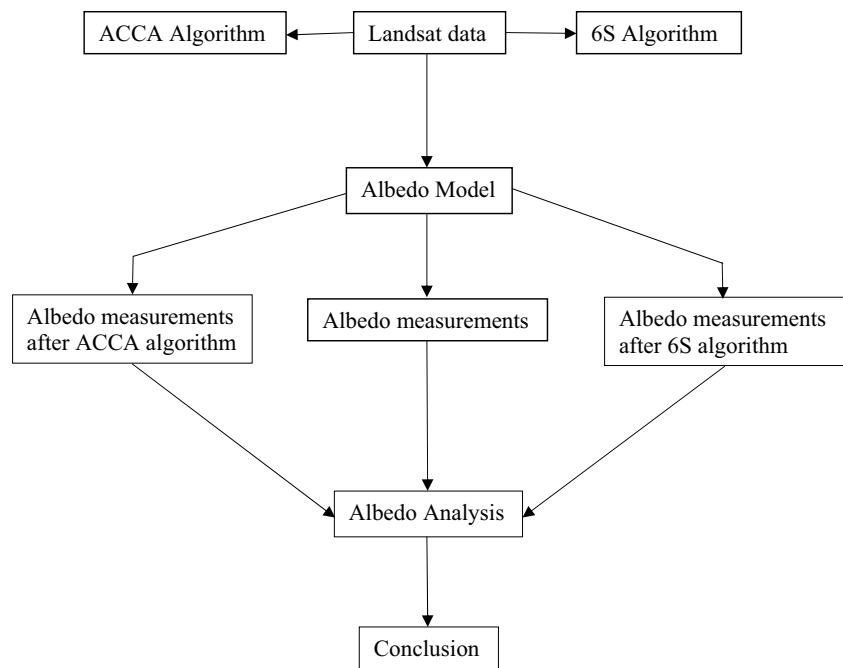
for the Landsat MSS, TM and ETM+ sensors data with no correction of terrain.

$$\rho_A = \pi L R^2 / \mu_{sun} S_o, \quad (2)$$

where ρ_A Planetary Albedo, π mathematical constant, L spectral radiance at the satellite, μ_{sun} solar zenith angle on the horizontal surface, S_o mean exo-atmospheric solar irradiance (Table 2), R Earth–Sun distance

4 Results and Discussion

Spectral albedo of visible bands and near-infrared bands are calculated with the criteria defined by the model. The albedo model is applied on the visible (band 1, band 2, and band 3) and near-infrared bands (band 4, band 5, and band 7) of TM (two images) and ETM+ (one image) data sets. The first TM image was captured on September 20, 1992 and the second image was taken on October 07, 1998 whilst the only ETM+ image was taken on October 07, 2000. Due to the non-availability of Landsat data for the same date and month over the study region the difference of 17 days in three images is compromised anticipating that it may not make much difference in calculating spectral albedo of snow. All images contain mix features including mountain peaks, valleys, coniferous and deciduous forests, water bodies and some extant of urban areas. Albedo ranges may vary

sharply because different features on the Earth reflect different energy. Normalized Difference Snow Index (NDSI) was applied to all images to extract snow bodies from other land surfaces. Albedo values were selected only for the snow cover area to analyze the reflectance difference within snow over the whole study area.

Snow albedo values for all three Landsat images over the study area are given in Table 3. First, we discuss the albedo values of the 1992 TM image with different bands. Band 3 shows maximum albedo value (0.736) among visible bands, whilst band 4 shows maximum albedo value (0.981) among infrared bands of TM. Similarly, for the year 1998 band 3 shows maximum albedo value (0.714) among visible bands, whilst band 4 shows maximum albedo value (0.936) among infrared bands of TM. Finally, for the year 2000 once again band 3 shows maximum albedo value (0.673) among visible bands, whilst band 4 shows maximum albedo value (0.913) among infrared bands of ETM+. The higher values of infrared band 4 for the entire dataset indicate the presence of fine grain size snow as well as the existence of non-Lambertian surfaces in the study area. Higher value of snow albedo in band 4 is also associated with minimum saturation in the particular spectral region. In addition, both TM and ETM+ visible bands are sensitive to small amount of dust (Dozier and Marks 1987) thereby indicate a significant decrease in albedo values. Results of the study also indicate (Table 3) that the snow albedo values slightly reduced when we apply ACCA algorithm as well as when we apply 6S model. Although this decrease is insignificant, further study is required to authenticate our findings. It is also evident from Table 3 that the snow albedo value is reducing as we move from the year 1992 to 2000 irrespective of bands and sensors data.

Snow cover albedo measurements using infrared band 4 (highest albedo among all bands of Landsat) of TM and ETM+ sensors for the years 1992, 1998, and 2000 are shown in Figs. 3a–c, 4a–c and 5a–c, respectively. Figures 3a, 4a and 5a show snow albedo values estimated directly from snow albedo model (Eq. 2) applied on TM and ETM+data. Similarly, Figs. 3b, 4b, and 5b highlight
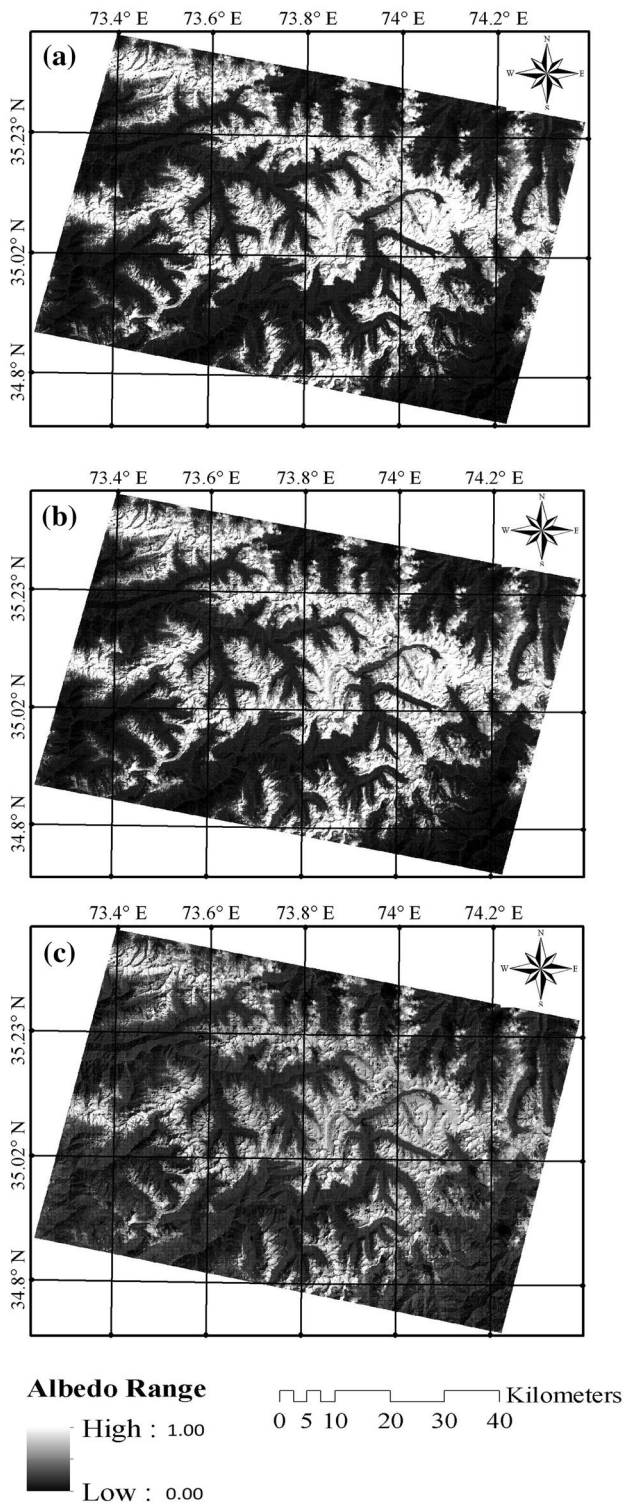
Table 2 Solar exo-atmospheric spectral irradiance (https://www.usgs.gov/media/images/effective-exo-atmospheric-solar-irradiance-esun)

Band	Landsat-2 (MSS)	Landsat-3 (MSS)	Landsat-5 (TM)	Landsat-7 (ETM+)
1	1829	1839	1957	1969
2	1539	1555	1826	1840
3	1268	1291	1554	1551
4	886.6	887.9	1036	1044
5			215.0	225.7
7			80.67	82.07

Table 3 Spectral albedo values retrieved from Landsat TM and ETM+ images

Band	TM 20 Sep 1992			TM 07 Oct 1998			ETM+ 07 Oct 2000		
	Albedo (Model)	Albedo (ACCA)	Albedo (6S)	Albedo (Model)	Albedo (ACCA)	Albedo (6S)	Albedo (Model)	Albedo (ACCA)	Albedo (6S)
1	0.563	0.544	0.532	0.434	0.427	0.418	0.414	0.404	0.402
2	0.637	0.621	0.615	0.621	0.616	0.605	0.607	0.603	0.601
3	0.744	0.736	0.721	0.714	0.706	0.701	0.673	0.668	0.664
4	0.989	0.981	0.973	0.957	0.942	0.936	0.913	0.911	0.908
5	0.583	0.563	0.552	0.611	0.608	0.601	0.631	0.626	0.623
7	0.615	0.611	0.601	0.645	0.631	0.625	0.684	0.681	0.675

Fig. 3 Albedo measurements in the infrared band 4 of TM sensor **a** direct albedo model, **b** albedo model after applying ACCA, and **c** albedo model after applying 6S for 20 September 1992

snow albedo values estimated after applying ACCA algorithm, whilst Figs. 3c, 4c and 5c illustrate snow albedo values estimated after applying 6S model on TM and ETM+
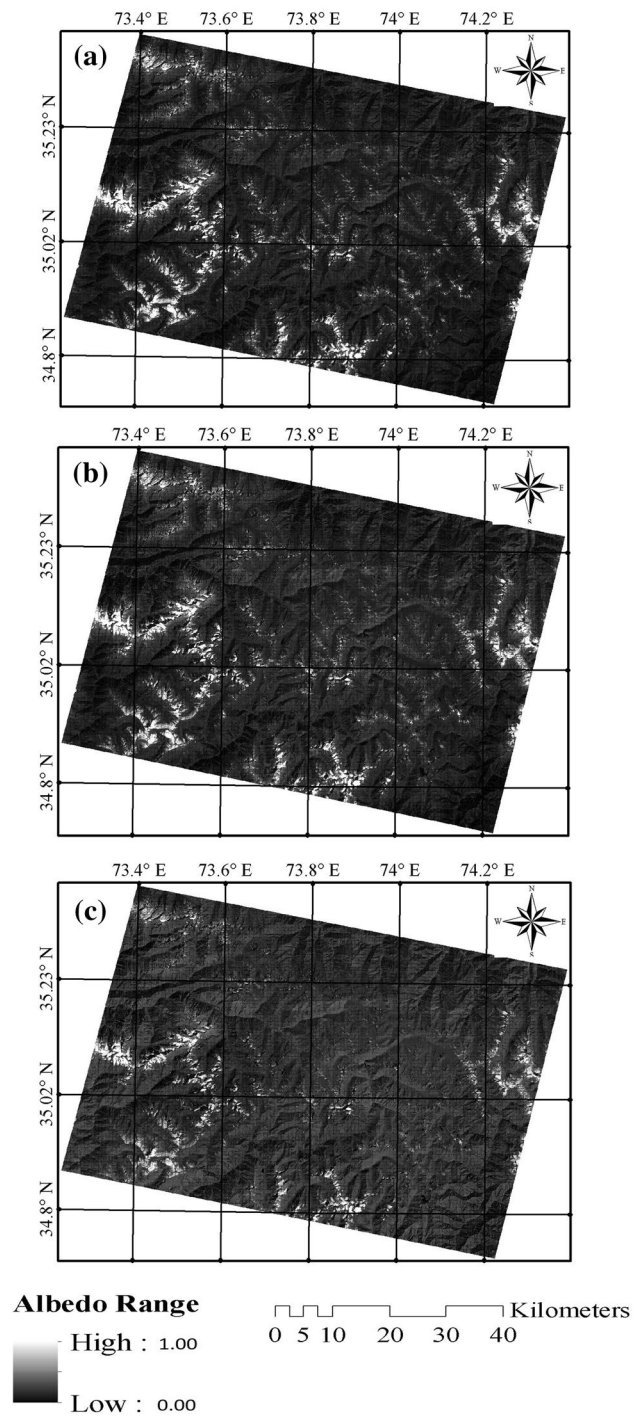
Fig. 4 Albedo measurements in the infrared band 4 of TM sensor **a** direct albedo model, **b** albedo model after applying ACCA, and **c** albedo model after applying 6S for 07 October 1998

data. It is evident from Figs. 3a–c, 4a–c and 5a–c that the snow albedo reflectance is highest when it is directly estimated from model (Eq. 2) followed by after applying ACCA and 6S models. These results are also verified by highest values of snow albedo estimation as given in
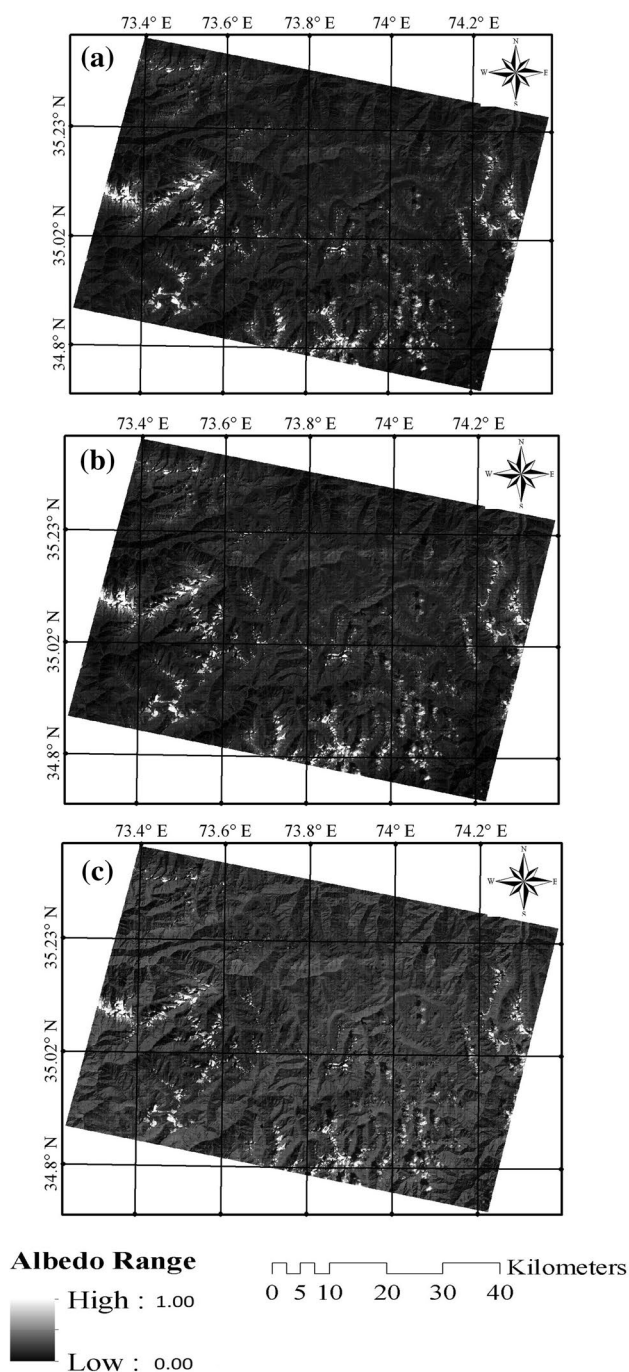
Albedo Range

High : 1.00

Low : 0.00

Kilometers
0 5 10   20   30   40

Fig. 5 Albedo measurements in the infrared band 4 of TM sensor **a** direct albedo model, **b** albedo model after applying ACCA, and **c** albedo model after applying 6S for 07 October 2001

Table 3. An interesting finding from Figs. 3, 4 and 5 is that the snow surface area in the study region has markedly reduced from the year 1992 to 1998, which further lost a number of snow traces in the year 2000. This is a very important finding both from climatological and hydrological point of view. However, to assess our results further we need to analyze meteorological data (temperature and

precipitation) retrieved from PMD stations in the vicinity of the study area.

4.1 Results Validation

For the purpose of uniformity, we have used temperature and precipitation data recorded in the study area (4 PMD stations) from the year 1954 to 2000. Annual average of temperature and precipitation from each station are used to calculate the temperature (Fig. 6a) and precipitation (Fig. 6b) anomalies in the study area. In the study area, the average estimated temperature is 15.86 °C whilst the average estimated precipitation is 246.8 mm. It is evident from Fig. 6a, b that since 1954 to 2000 the temperature has a decreasing trend whilst precipitation has an increasing trend in the study area. The highest (lowest) temperature and precipitation anomalies in the study area are observed for the years 1971 (1957) and 1996 (1977), respectively. In the current study, since we have used Landsat data for the years 1992, 1998, and 2000 therefore, we have also analyzed temperature and precipitation anomalies from the year 1990 to 2000 (Fig. 7a, b). Our analysis indicates that in the study area temperature (Fig. 7a) has an increasing trend whilst precipitation (Fig. 7b) has a decreasing trend during the said period. The average estimated temperature from the years 1990 to 2000 in the study region is 15.87 °C whilst the average estimated rainfall is 262.6 mm. The highest (lowest) temperature and precipitation anomalies in the study area for the study period are observed for the years 1990 (1996) and 1996 (2000), respectively. It is noted that temperature shows negative anomaly for 4 years (1992, 1993, 1995, and 1996) and positive anomaly for the remaining 7 years in the study area from years 1990 to 2000. Similarly, precipitation shows positive anomaly for 5 years (1992, 1993, 1994, 1996, and 1999) and negative anomaly for the remaining 6 years in the study area from years 1990 to 2000. It is also noted that temperature has a positive anomaly after the year 1996, which is one of the most important reason that why the snow area has been reduced in the study region (Figs. 4, 5) during the study period.

5 Conclusions

The objective of this study is to analyze spectral albedo of snow cover in the northern region of Pakistan using Landsat satellite data. Snow spectral albedo is estimated directly as well as after applying ACCA and 6S models on Landsat data. One of the main advantages of using satellite data for the estimation of spatially variable features like snow cover is large area coverage (including physically unaccusable areas), near real-time, and low cost. However, the rugged terrain pose some problems related to topography,
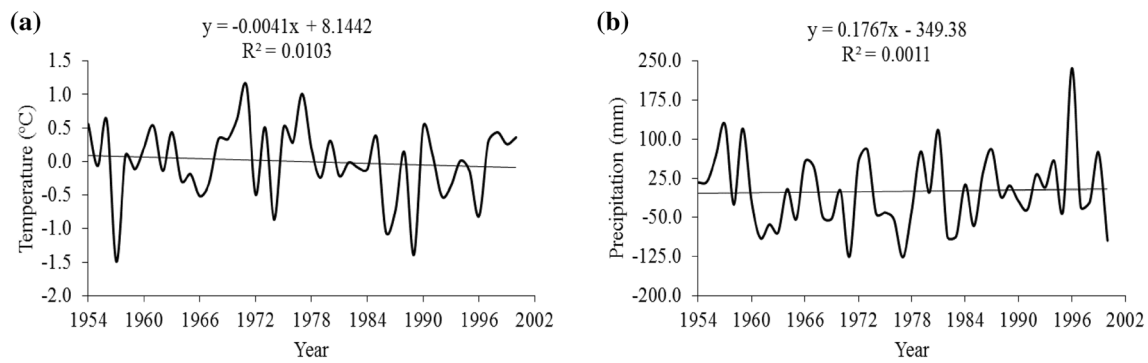
(a)

y = -0.0041x + 8.1442
R² = 0.0103

(b)

y = 0.1767x - 349.38
R² = 0.0011

Fig. 6 Anomalies in the study region from the year 1954 to 2000 **a** temperature and **b** precipitation

(a)

y = 0.0289x - 57.571
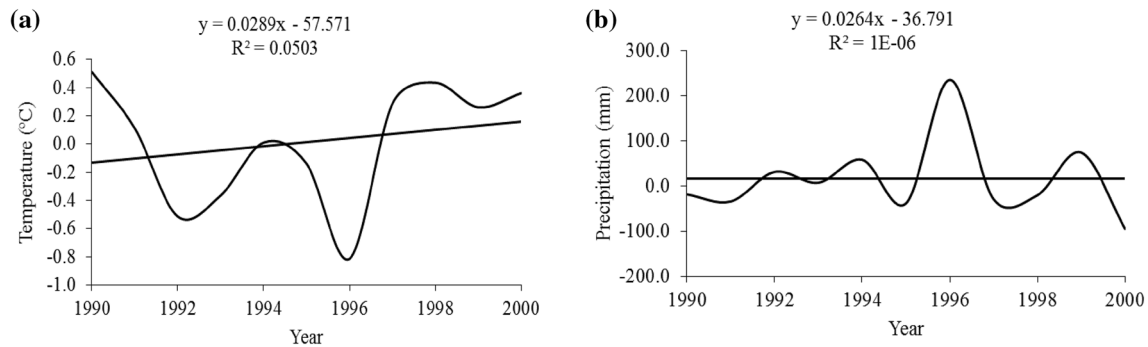R² = 0.0503

(b)

y = 0.0264x - 36.791
R² = 1E-06

Fig. 7 Anomalies in the study region from the year 1990 to 2000 **a** temperature and **b** precipitation

such problems are overcome, in part by eliminating the dark edges and shadows covering a nominal portion of the satellite imagery.

The results of the study indicate that the snow spectral albedo estimated by directly using Eq. 2 has the highest value for all bands of Landsat data while the values slightly decreasing when we apply ACCA and 6S algorithm (Table 3) for the study period. One reason for slightly decreased spectra albedo values after applying ACCA algorithm is the removal of cloud cover from the Landsat data. Although the utmost care has been taken to choose only cloud-free imagery but similar reflectance of snow and cloud in an image can sometime hampered the visual interpretation to omit cloud cover, which consequently is removed using ACCA algorithm. Since clouds are formed from frozen droplet they contributed to the reflectance values and thereby may give some erroneous results. It is recommended that further research is needed to analyze the ACCA and 6S model impacts in the study region. The results of the study also show that irrespective of the measurement method of snow spectral albedo, Landsat band 1 has the lowest value of albedo followed by band 5, band 7, band 2, and band 3 whilst highest value is obtained using band 4. The percentage change in snow spectral albedo from lowest value (band 1) to highest value (band 4) is 42.6% for the year 1992,

52.3% for the year 1998, and 49.9% for the year 2000. This can clearly be associated with snow contamination as visible band is more sensitive to dust particles present in snow surface and thereby reducing the spectral signature.

Another important finding of the current research is the reduction of snow surface area in the study region. Although, 1992 Landsat image is earlier (20 September) as compared to remaining two Landsat images (07 October) it is believed that the difference of 17 days has no impact in the reduction of snow surface area in the study region. Our analysis on meteorological data reveals that due to the increase in average annual temperature and a decrease in average annual precipitation the snow area has been reduced. This is very alarming for climatologist as well as for hydrologists. However, further study is required to better understand the snow behavior in the study region. It is concluded that the albedo variations in snow cover region of Northern Pakistan are significant and needed to be taken into considerations while calculating surface radiation balance and developing regional climate models. In addition, a timely prepared database on snow albedo information can be very useful for predicting snow melt runoff during spring and summer seasons.

References

Bhutiyani M, Kale V, Pawar N (2010) Climate change and the precipitation variations in the northwestern Himalaya: 1866–2006. Int J Climatol 30:535–548

Butt MJ (2012) Characteristics of snow cover in the Hindukush, Karakoram and Himalaya (HKH) region using Landsat satellite data. Hydrological Processes 26:3689–3698. https://doi.org/10.1002/hyp.8375

Butt MJ (2013) Exploitation of Landsat data for Snow Zonation Mapping in Hindukush, Karakoram and Himalaya (HKH) Region of Pakistan. Hydrol Sci J 58(5):1088–1096. https://doi.org/10.1080/02626667.2013.799774

Chander G, Markham BL (2003) Revised Landsat-5 TM radiometric calibration procedures and postcalibration dynamic ranges. IEEE Trans Geosci Remote Sens 41(11):2674–2677

Chander G, Markham BL, Helder DL (2009) Summary of current radiometric calibration coefficients for Landsat MSS, TM, ETM+, and EO-1 ALI sensors. Remote Sens Environ 113:893–903

Cheng Q, Shen H, Zhang L, Yuan Q, Zeng C (2014) Cloud removal for remotely sensed images by similar pixel replacement guided with a spatio-temporal MRF model. ISPRS J Photogramm Remote Sens 92:54–68

Csiszar I, Gutman G (1999) Mapping global land surface albedo from NOAA AVHRR. J Geophys Res 104:6215–6228

Déry SJ, Brown RD (2007) Recent Northern Hemisphere snow cover extent trends and implications for the snow-albedo feedback. Geophys Res Lett. https://doi.org/10.1029/2007gl031474

Dimri AP, Chevuturi A (2016) Western disturbances—an Indian meteorological perspective. Springer, Switzerland

Dimri AP, Dash SK (2012) Wintertime climatic trends in the western Himalayas. Clim Change 111(3–4):775–800

Dobhal DP, Mehta M, Srivastava D (2013) Influence of debris cover on terminus retreat and mass changes of Chorabari Glacier, Garhwal region, central Himalaya, India. J Glaciol 59(217):961–971

Dozier J (1989) Spectral signature of alpine snow cover from the Landsat Thematic Mapper. Remote Sens Environ 28:9–22

Dozier J, Marks D (1987) Snow mapping and classification from Landsat Thematic Mapper. Ann Glaciol 9:97–103

Fletcher CG, Kushner PJ, Hall A, Qu X (2009) Circulation responses to snow albedo feedback in climate change. Geophys Res Lett 36:L09702

Gao Y, Xie H, Lu N, Yao T, Liang T (2010) Toward advanced daily cloud-free snow cover and snow water equivalent products from Terra-Aqua MODIS and Aqua AMSR-E measurements. J Hydrol 385(1–4):23–35

Graversen RG, Wang M (2009) Polar amplification in a coupled climate model with locked albedo. Clim Dyn 33:629–643

Greuell W, de Wildt MD (1999) Anisotropic reflection by melting glacier ice: measurements and parameterizations in Landsat TM bands 2 and 4. Remote Sens Environ 70(3):265–277

Grünewald T, Bühler Y, Lehning M (2014) Elevation dependency of mountain snow depth. Cryosphere 8(6):2381–2394

Gupta RP, Ghosh A, Haritashya UK (2007) Empirical relationship between near-IR reflectance of melting seasonal snow and environmental temperature in a Himalayan basin. Remote Sens Environ 107:402–413

Gurung DR, Maharjan SB, Shrestha AB, Shrestha MS, Bajracharya SR, Murthy MSR (2017) Climate and topographic controls on snow cover dynamics in the Hindu Kush Himalaya. Int J Climatol 37(10):3873–3882

Haeberli W (2004) Glaciers and ice caps: historical background and strategies of world-wide monitoring. In: Bamber JL, Payne AJ (eds) Mass balance of the cryosphere: observations and modelling of contemporary and future change. Cambridge University Press, Cambridge, pp 559–578

Haeberli W, Whiteman C, Shroder JF (eds) (2014) Snow and ice-related hazards, risks and disasters. Academic Press, Waltham

Hall DK, Martinec J (1985) Remote sensing of ice and snow. Chapman and Hall, London, p 189

Hall DK, Riggs GA, Foster JL, Kumar SV (2010) Development and evaluation of a cloud-gap-filled MODIS daily snow-cover product. Remote Sens Environ 114(3):496–503

Hu B, Lucht W, Strahler AH (1999) The interrelationship of atmospheric correction of reflectances and surface BRDF retrieval: a sensitivity study. IEEE Trans Geosci Remote Sens 36:724–738

Immerzeel WW, Van Beek LP, Bierkens MF (2010) Climate change will affect the Asian water towers. Science 328(5984):1382–1385

IPCC (2013) Summary for policymakers. In: Stocker TF, Qin D, Plattner G-K, Tignor M, Allen SK, Boschung J, Nauels A, Xia Y, Bex V, Midgley PM (eds) Climate change 2013: the physical science basis. contribution of working group I to the fifth assessment report of the intergovernmental panel on climate change. Cambridge University Press, Cambridge. https://doi.org/10.1017/cbo9781107415324

Joshi R, Kumar K, Pandit J, Palni LMS (2015) Variations in the seasonal snow cover area (SCA) for Upper Bhagirathi Basin, India. In: Kumar K, Palni L (eds) JoshiR. Dynamics of climate change and water resources of Northwestern Himalaya. Springer, Cham, pp 9–21

Kääb A, Paul F, Maisch M, Hoelzle M, Haeberli W (2002) The new remote-sensing-derived Swiss glacier inventory: II. First results. Ann Glaciol 34:362–366

Kaser G, Großhauser M, Marzeion B (2010) Contribution potential of glaciers to water availability in different climate regimes. Proc Natl Acad Sci 107:20223–20227

Kasturirangan K, Navalgund RR, Ajai (2013) Observed changes in the Himalayan–Tibetan glaciers. Fate of Mountain Glaciers in the Anthropocene Pontifical Academy of Sciences, Vatican City

Khromova TE, Dyurgerov M, Barry RG (2003) Late-twentieth century changes in glacier extent in the Ak-shirak Range, Central Asia, determined from historical data and ASTER imagery. Geophys Res Lett 30(16):1863

Knap WH, Brock BW, Oerlemans J, Willis IC (1999) Comparison of Landsat TM derived and ground-based albedos of Haut Glacier d'Arolla, Switzerland. Int J Remote Sens 20(17):3293–3310

Kukla GJ, Kukla HJ (1974) Incresead surface albedo in the northern hemisphere. Science 189:709–714

Kulkarni AV, Rathore BP, Singh SK, Bahuguna IM (2011) Understanding changes in the Himalayan cryosphere using remote sensing techniques. Int J Remote Sens 32(3):601–615

Li Z, Garand L (1994) Estimation of surface albedo from space: a parameterization for global application. J Geophys Res 99:8335–8350

Li X, Shen H, Zhang L, Zhang H, Yuan Q, Yang G (2014) Recovering quantitative remote sensing products contaminated by thick clouds and shadows using multitemporal dictionary learning. IEEE Trans Geosci Remote Sens 52(11):7086–7098

Liang S, Fang H, Chen M (2001) Atmospheric correction of Landsat ETM+ land surface imagery-part I: methods. IEEE Trans Geosci Remote Sens 39(11):2490–2498

López-Burgos V, Gupta HV, Clark M (2013) Reducing cloud obscuration of MODIS snow cover area products by combining spatio-temporal techniques with a probability of snow approach. Hydrol Earth Syst Sci 17(5):1809–1823

Maisch M (2000) The long-term signal of climate change in the Swiss Alps: glacier retreat since the end of the Little Ice Age and future ice decay scenarios. Geografia Fisica e Dinamica Quaternaria 23(2):139–152

Negi HS, Shekhar MS, Gusain HS, Ganju A (2018) Winter climate and snow cover variability over north-west Himalaya. In: Goel P, Ravindra R, Chattopadhyay S (eds) Science and geopolitics of the white world. Springer, Cham, pp 127–142

Oleson KW, Bonan GB, Schaaf CB, Gao F, Jin Y, Strahler AH (2003) Assessment of global climate model land surface albedo using MODIS data. Geophys Res Lett. https://doi.org/10.1029/2002gl016749

Ollinger SV, Richardson AD, Martin ME, Hollinger DY, Frolking SE, Reich PB et al (2008) Canopy nitrogen, carbon assimilation and albedo in temperate and boreal forests: functional relations and potential climate feedbacks. Proc Natl Acad Sci USA 105:19335–19340

Parajka J, Pepe M, Rampini A, Rossi S, Blöschl G (2010) A regional snow-line method for estimating snow cover from MODIS during cloud cover. J Hydrol 381(3–4):203–212

Paudel KP, Andersen P (2011) Monitoring snow cover variability in an agropastoral area in the Trans Himalayan region of Nepal using MODIS data with improved cloud removal methodology. Remote Sens Environ 115(5):1234–1246

Paul F, Huggel C, Kääb A (2004a) Combining satellite multispectral image data and a digital elevation model for mapping of debris-covered glaciers. Remote Sens Environ 89(4):510–518

Paul F, Kääb A, Maisch M, Kellenberger T, Haeberli W (2004b) Rapid disintegration of Alpine glaciers observed with satellite data. Geophys Res Lett 31(21):L21402

Qu X, Hall A (2007) What controls the strength of snow-albedo feedback? J Clim 20:3971–3981

Rathore BP, Singh SK, Jani P, Bahuguna IM, Brahmbhatt R, Rajawat AS, Randhawa SS, Vyas A (2018) Monitoring of snow cover variability in Chenab Basin using IRS AWiFS sensor. J Indian Soc Remote Sens. https://doi.org/10.1007/s12524-018-0797-8

Robinson N, Regetz J, Guralnick RP (2014) EarthEnv-DEM90: a nearly-global, voidfree, multi-scale smoothed, 90 m digital elevation model from fused ASTER and SRTM data. ISPRS J Photogramm Remote Sens 87:57–67

Roesch A, Schaaf CB, Gao F (2004) Use of Moderate-Resolution Imaging Spectroradiometer bidirectional reflectance distribution function products to enhance simulated surface albedos. J Geophys Res 109(D12):D12105

SAC (2016) Monitoring snow and glaciers of Himalayan region. Space Applications Centre, ISRO, Ahmedabad (ISBN: 978-93-82760-24-5)

Schaaf CL, Martonchik J, Pinty B, Govaerts Y, Gao F, Lattanzio A et al (2008) Retrieval of surface albedo from satellite sensors. In: Liang S (ed) Advances in land remote sensing: system, modeling, inversion and application. Springer, Dordrecht, pp 219–243

Shukla S, Kansal ML, Jain SK (2017) Snow cover area variability assessment in the upper part of the Satluj river basin in India. Geocarto Int 32(11):1285–1306 (Springer 978-1-4020-6449-4)

Smith T, Bookhagen B (2018) Changes in seasonal snow water equivalent distribution in High Mountain Asia (1987 to 2009). Sci Adv 4(1):e1701550

Snehmani, Singh MK, Gupta RD, Bhardwaj A, Joshi PK (2015) Remote sensing of mountain snow using active microwave sensors: a review. Geocarto Int 30(1):1–27

Snehmani, Dharpure JK, Kochhar I, Hari Ram RP, Ganju A (2016) Analysis of snow cover and climatic variability in Bhaga basin located in western Himalaya. Geocarto Int 31(10):1094–1107

Snyder JP (1987). Map projections. A working manual. US Geological Survey professional paper 1395. United States Geological Survey, Reston

Souma K, Wang YQ (2010) A comparison between the effects of snow albedo and infiltration of melting water of Eurasian snow on East Asian summer monsoon rainfall. J Geophys Res Atmos 115:D02115

Srinivasulu J, Kulkarni AV (2004) Estimation of spectral reflectance of snow from IRS-1D LISS-III sensor over the Himalayan terrain. Proc Indian Acad Sci Earth Planet Sci 113(1):117–128

Stigter EE, Wanders N, Saloranta TM, Shea JM, Bierkens MF, Immerzeel WW (2017) Assimilation of snow cover and snow depth into a snow model to estimate snow water equivalent and snowmelt runoff in a Himalayan catchment. Cryosphere 11(4):1647–1664

Tekeli AE, Sönmez I, Erdi E (2016) Snow-covered area determination based on satellitederived probabilistic snow cover maps. Arab J Geosci 9(3):198

Thayyen RJ, Dimri AP (2018) Slope environmental lapse rate (SELR) of temperature in the monsoon regime of the western Himalaya. Front Environ Sci 6:42

Thayyen RJ, Gergan JT (2010) Role of glaciers in watershed hydrology: a preliminary study of a" Himalayan catchment". Cryosphere 4(1):115–128

Tian Y, Dickinson RE, Zhou L, Myneni RB, Friedl M, Schaaf CB et al (2004) Land boundary conditions from MODIS data and consequences for the albedo of a climate model. Geophys Res Lett. https://doi.org/10.1029/2003gl019104

Viterbo P, Betts AK (1999) Impact on ECMWF forecasts of changes to the albedo of the boreal forests in the presence of snow. J Geophys Res 104:27803–27810

Wang W, Huang X, Deng J, Xie H, Liang T (2014) Spatio-temporal change of snow cover and its response to climate over the Tibetan Plateau based on an improved daily cloudfree snow cover product. Remote Sens 7(1):169–194

Xiao X, Shen Z, Qin X (2001) Assessing the potential of vegetation sensor data for mapping snow and ice cover: a Normalised Difference Snow and Ice Index. Int J Remote Sens 22:2479–2487

Yang FL, Kumar A, Wang WQ, Juang HMH, Kanamitsu M (2001) Snow- lbedo feedback and seasonal climate variability over North America. J Clim 14:4245–4248

Zhang Y, Wang X, Chen Y (2012) An improved 6S code for atmospheric correction based on water vapor content. Adv Remote Sens 1(1):14–18. https://doi.org/10.4236/ars.2012.11002